Research on Modeling and Compensation Methods of Dip and Azimuth Errors of Downhole Inclinometer

Wenming Xue[1, a], He Zhang[1, b]

[1]School of Southwest Petroleum University, Chengdu 610500, China.

[a]652359347@qq.com, [b]11413943@qq.com

Abstract

For the downhole tilt-while-drilling technology, the error caused by the inertial device itself and the interference caused by the harsh downhole conditions are complex. Error compensation is a key factor affecting the accuracy of the measurement. Based on explaining the principle of inclinometer and analyzing the influencing factors of inclinometer error, this paper proposes a compensation method based on RBF neural network for tilt and azimuth errors and a compensation method based on the smallest tilt and azimuth errors. The output of the accelerometer is used as the input of the neural network and the inclination is used as the output to train the RBF network. The advantage of this method is that it does not need to model the sensor mathematically, neither does it need to know the form of the fitted function. Larger errors. In order to solve the shortcomings of the poor generalization performance of RBF and minimize the inclination and azimuth errors, the error compensation can be realized by directly minimizing the inclination and azimuth errors. These two methods are used to conduct MATLAB simulation experiments, and the simulation results are compared with the errors. The results show that the compensation method based on the smallest inclination and azimuth errors has good fitting performance, the compensation of the backward tilt and azimuth errors is effectively suppressed, and the compensation accuracy is high , Each index is better than RBF neural network method.

Keywords

Inclinometer while drilling; Error compensation; RBF neural network; MATLAB simulation.

1. Introduction

With the large-scale development of horizontal wells and extended-reach wells in the field of oil and gas extraction, a tilt-while-drilling instrument capable of measuring drilling trajectories in real time is of great significance for improving the accuracy of wellbore trajectory control and improving the efficiency of oil and gas extraction. Wellbore profile design, drill string design, and wellbore trajectory control are important factors affecting horizontal wells and extended reach wells[1]. As a real-time monitoring system for downhole drilling tools, the LWD instrument can accurately measure the borehole geometric parameters (wellbore, azimuth, tool face, etc.)[2] during the drilling process, so that technicians can know the direction of the downhole drilling tool And working attitude to control the trajectory of the wellbore.

However, in the use of the inclinometer, as time goes by and the number of downhole uses increases, the performance of the instrument and the electronic circuit in the instrument will change. This requires the instrument to be calibrated and data recorded within a certain period of time. To check the performance of the instrument. This article studies the installation error of the inclinometer, achieves the goal of improving the accuracy of the inclinometer, reduces the cost of inclinometer calibration, increases the calibration rate, and provides a research idea for the cost and efficiency of inclinometer calibration.

The inclinometer measurement module consists of three acceleration sensors and three magnetoresistive sensors, which are orthogonal to each other in space position. During the attitude measurement process, the acceleration sensor and the fluxgate sensor detect the gravity acceleration

component and the geomagnetic field component on the X, Y, and Z axes, respectively, and are used to extract the attitude information of the drill pipe borehole. However, due to the influence of the processing and installation errors of the sensor while measuring the inclination while drilling, the well deviation, azimuth and tool face angle measured by it have large errors, which in turn affects the precision of the drilling tool to control the well deviation[3].

By analyzing the attitude measurement principle and mathematical model of the inclinometer, this paper studies in detail the current inclinometer error calibration models and methods, and proposes an inclination and azimuth error compensation method based on the RBF neural network and a compensation based on the smallest inclination and azimuth error. Method, and used MATLAB to carry out simulation analysis and error analysis, and compared the advantages and disadvantages of these two methods and the existing problems.

2. Analysis of Inclinometer Principle and Influencing Factors of Error

2.1 Measuring principle of inclinometer

The installation positions of the three acceleration sensors and three magnetoresistive sensors in the inclinometer are shown in Fig 1.

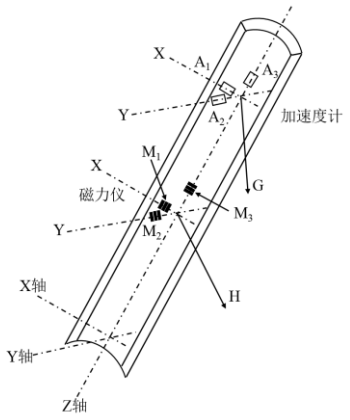

Fig 1 Installation positions of three acceleration sensors and three magnetoresistive sensors

On the three orthogonal acceleration sensors, the gravity field components of the gravity acceleration G are respectively represented as G_x, G_y, and G_z; on the three orthogonal magnetoresistive sensors, the components of the geomagnetic field H are respectively represented as H_x, H_y, and H_z, respectively. G_z indicates the direction of the axis of the gravity accelerometer down the wellbore axis. The directions of G_x, G_y are orthogonal to G_z and meet the right-hand spiral rule. The directions of H_x, H_y are the same as the directions of G_x, G_y. The H_z axis output signals from the gravity acceleration sensor and the magnetoresistive sensor are amplified, A/D converted and sent to the central processor for calculation. The well deflection angle, azimuth angle, and tool face angle can be calculated[4].

The reference vector uses gravity acceleration and geomagnetic field strength to establish the attitude reference of the borehole[5][6]. Let $OX_NY_NZ_N$ be the local reference coordinate system and $OX_PY_PZ_P$ be the probe coordinate system. And define:

$$A_Z \xrightarrow{Around\ Z_N} Magnetic\ azimuth$$

$$INC \xrightarrow{Around\ Y'} Well\ angle$$

$$TF \xrightarrow{Around\ Z_P} Tool\ face\ angle$$

Let the cosine array of the direction between the two coordinate systems be C_N^P, then the gravity acceleration has the following relationship between the projections of the two coordinate systems:

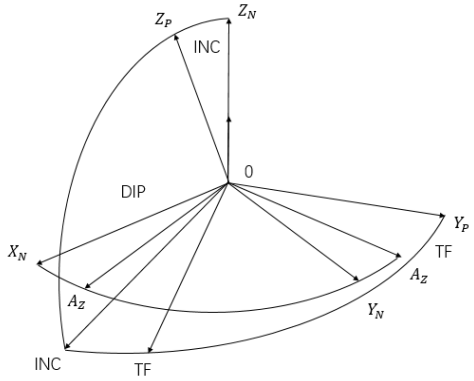

Fig 2 Rotation relationship between $OX_NY_NZ_N$ and $OX_PY_PZ_P$

$$\begin{bmatrix} G_{XP} \\ G_{YP} \\ G_{ZP} \end{bmatrix} = C_N^P \begin{bmatrix} G_{XN} \\ G_{YN} \\ G_{ZN} \end{bmatrix} = C_N^P \begin{bmatrix} 0 \\ 0 \\ G \end{bmatrix}$$

$$= \begin{bmatrix} cosTF & sinTF & 0 \\ -sinTF & cosTF & 0 \\ 0 & 0 & 1 \end{bmatrix} \begin{bmatrix} cosINC & 0 & -sinINC \\ 0 & 1 & 0 \\ sinINC & 0 & cosINC \end{bmatrix} \begin{bmatrix} cosA_Z & sinA_Z & 0 \\ -sinA_Z & cosA_Z & 0 \\ 0 & 0 & 1 \end{bmatrix} \begin{bmatrix} 0 \\ 0 \\ G \end{bmatrix} \tag{1}$$

Where: G_{XP}, G_{YP}, G_{ZP} are the projections of gravity acceleration in the inclinometer coordinate system; G_{XN}, G_{YN}, and G_{ZN} are the projections of gravity acceleration in the reference coordinate system; G is the value of gravity acceleration, which is obtained by expansion:

$$C_N^P = \begin{bmatrix} cosTFcosINCcosA_Z - sinTFsinA_Z & cosTFcosINCsinA_Z + sinTFcosA_Z & -cosTFsinINC \\ -sinTFcosINCcosA_Z - cosTFsinA_Z & -sinTFcosINCsinA_Z + cosTFcosA_Z & sinTFsinINC \\ sinINCcosA_Z & sinINCsinA_Z & cosINC \end{bmatrix} \tag{2}$$

The geomagnetic field strength has the following relationship between the projections of the two coordinate systems:

$$\begin{bmatrix} B_{XP} \\ B_{YP} \\ B_{ZP} \end{bmatrix} = C_N^P \begin{bmatrix} B_{XN} \\ B_{YN} \\ B_{ZN} \end{bmatrix} = C_N^P \begin{bmatrix} BcosDIP \\ 0 \\ -BsinDIP \end{bmatrix} \tag{3}$$

In the formula: B_{XP}, B_{YP}, B_{ZP} are the projections of the geomagnetic field intensity on the inclinometer coordinate system; B_{XN}, B_{YN}, B_{ZN} are the projections of the geomagnetic field intensity on the reference coordinate system; B is the geomagnetic field intensity value; DIP is the local geomagnetic inclination angle.

It is easy to get from (1), (2), (3):

$$INC = tg^{-1}\left(\frac{\sqrt{G_{XP}^2 + G_{YP}^2}}{G_{ZP}}\right) \tag{4}$$

$$TF = tg^{-1}\left(\frac{-G_{YP}}{G_{XP}}\right) \tag{5}$$

$$AZ = tg^{-1}\left[-\frac{B_{XP}sinTF + B_{YP}cosTF}{(B_{XP}cosTF - B_{YP}sinTF)cosINC + B_{ZP}sinINC}\right] \tag{6}$$

According to formulas (4), (5), and (6), as long as the gravity acceleration and geomagnetic field strength components along the axes of the inclinometer can be accurately measured, the well deviation, azimuth, and tool face angle can be calculated.

2.2 2.2 Analysis of influencing factors of inclinometer error

There are many factors that affect the measurement accuracy of the inclinometer, such as the measurement error of the sensor data, the installation error of the sensor in the instrument coordinate system, the temperature drift error, and the magnetic interference of the borehole environment.

(1) Installation error

The installation error is mainly composed of the misalignment angle between the sensor's sensitive axis and the inclinometer coordinate system, the processing error of the inclinometer structure, and the installation error of the sensor on the inclinometer[7]. As mentioned earlier, three accelerometers and three magnetic flux doors are installed orthogonally on the inclinometer, and they are installed in the T-slot orientation on the inclinometer. As shown in Fig 3, taking the accelerometer as an example, the installation error on the inclinometer is plotted, where XYZ is the inclinometer coordinate system and $X'Y'Z'$ is the direction of the three sensitive axes.

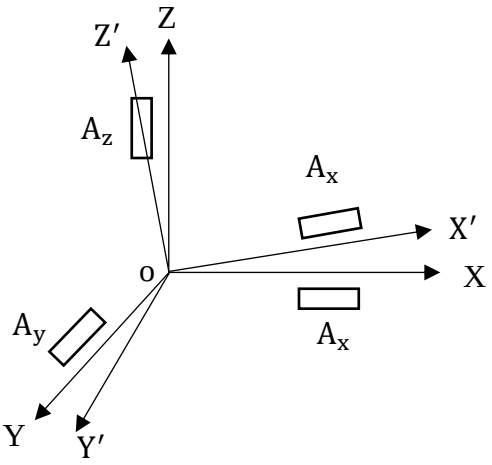

Fig 3 Installation error of accelerometer on inclinometer position

(2) Temperature drift error

Accelerometer sensors and fluxgate sensors are sensitive measuring devices, and their output signals change linearly with temperature[8]. The main reasons for the temperature error of the accelerometer sensor are:

① As the temperature increases, the torque coil increases and the magnetic flux increases, which increases the non-linear error of the accelerometer sensor;② The thermal imbalance of the quartz flexible accelerometer will slightly deform the mechanical arm, cause the signal zero point to drift, and change the zero point deviation value;③ The temperature gradient inside the accelerometer component will change the viscosity of the air, making the zero deviation of the accelerometer slightly change.

The main reasons for the temperature error of the fluxgate sensor are:

① As the temperature increases, the magnetic flux of the core material will change slightly, which increases the non-linear error of the fluxgate sensor;② The internal thermal compensation balance of the fluxgate sensor may cause slight changes in the external magnetic and excitation saturation.

(3) Processing error

This kind of error includes two contents: ① errors caused by defects in transmission and recording methods; ② errors caused by incomplete data processing[9]. Now inclinometers are basically electronic products, using high-performance microprocessors and AD converter chips, to complete

data acquisition, storage and reading under program control, reducing human participation, and its accuracy mainly depends on the position of AD With the rapid development of microelectronic technology, this error can be controlled at a very low level.

In terms of signal transmission, the inclinometer has two transmission modes: wireless and wired. The signal transmission of the wired system is simple and fast, and the bit error rate is low. In the wireless system, the mud pulse mode information exchange speed is slow, and the design of the receiving and sending system is complicated. In order to reduce the bit error rate, various error detection methods are used. Both transmission systems reduce transmission errors to negligible levels.

(4) Sensor measurement error

This error is mainly caused by the flaws in the precision processing of the sensor itself and the flaws in principle. The harsh working environment of drilling instruments not only tests the reliability of the instrument itself, but also involves various errors related to the environment.

3. Model and Simulation of Error Calibration Based on RBF Network

3.1 RBF network foundation

In 1988, Broomhead and Lowe published a paper that initially discussed the different characteristics of RBF for neural network design and traditional interpolation. Then they proposed a three-layer RBF neural network. They were the first to use RBF for neural network design[10]. Later in 1989, Moody and Darken also published an article that proposed a neural network with local response characteristics, namely the radial basis function neural network structure (RBF). At the same time, they also proposed a training method for the RBF network[11].

RBF is a three-layer forward neural network, similar to a multi-layer forward neural network, including an input layer, a hidden layer, and an output layer. Among them, the input layer is composed of signal source nodes; the second layer is the hidden layer. The number of hidden layer elements is determined according to the needs of the described problem. The radial basis function is a radial symmetry and attenuation relative to the center point Non-negative linear local response function, the specific local response is reflected in the conversion from the visible layer to the hidden layer, which is different from other networks; the third layer is the output layer, which responds to the role of the input mode. The role of the input layer is only to transmit signals. The connection between the input layer and the hidden layer can be regarded as a connection with a weight of 1. Because the output layer and the hidden layer perform different tasks, their learning strategies are also different. The role of the output layer is to adjust the linear weights. The learning strategy it uses is linear optimization, which has the advantage of faster learning speed. The role of the hidden layer is to adjust the parameters of the activation function (Green function, Gaussian function). The strategy is non-linear optimization, so the learning speed is slower. That is, the transformation from input space to hidden layer space is non-linear, while the transformation from hidden layer space to output layer space is linear. The flow chart is shown in Fig 4.

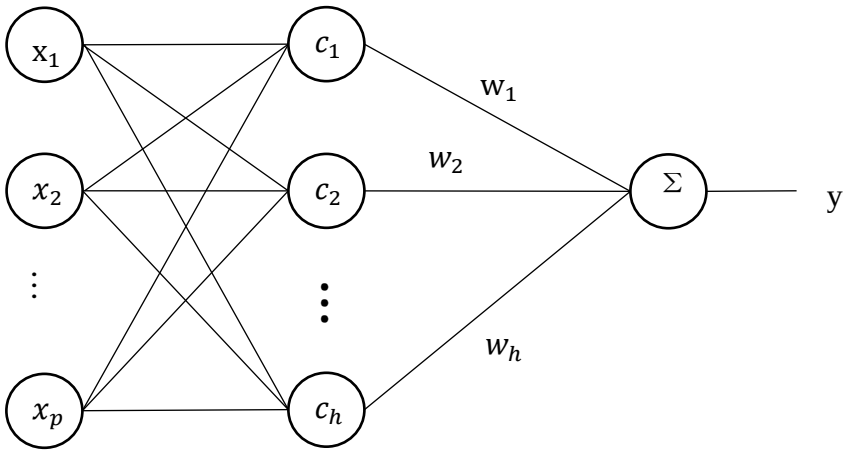

Fig 4 RBF neural network flowchart

According to the analysis of the RBF network structure, the basic idea of the RBF network[12] is: use RBF as the "base" of the hidden layer unit to form the hidden layer space, so that the input vector can be directly mapped to the hidden layer space without Requires weight connection. According to Cover's theorem, data that cannot be divided in low-dimensional space is more easily divided in high-dimensional space. In other words, the role of the hidden layer of the RBF network is to map the input of the low-dimensional space to a high-dimensional space through a non-linear function, and then fit the curve in this high-dimensional space. This is equivalent to finding a surface in the implicit high-dimensional space that is most suitable for training data. This is different from ordinary multilayer perceptron (MLP).

When the RBF center point is determined, the mapping relationship is also determined. The mapping from the hidden layer space to the output space is linear, that is, the output of the network is a linear weighted sum of the outputs of the hidden layer units, and the weight here is the adjustable parameter of the network. Among them, the function of the hidden layer is to map the vector from p in the low dimension to h in the high dimension, so that the case of low-dimensional linear inseparability becomes high-dimensional linearly separable, which is mainly the idea of the kernel function. Therefore, the mapping of the network from input to output is non-linear, and the output of the network is linear to the adjustable parameters. The weights of the network can be directly solved with linear equations, which greatly speeds up the learning speed and avoids local minimum problems.

The activation function of an RBF network is usually expressed as:

$$R(x_p - c_i) = \exp(-\frac{1}{2\sigma^2}\|x_p - c_i\|^2) \tag{7}$$

Among them: x_p represents the p-th input sample; c_i represents the i-th center point; h represents the number of nodes in the hidden layer; n represents the number of samples or classifications output. According to the structure of the RBF network, the output of the network can be obtained as:

$$y_j = \sum_{i=1}^{h} w_{ij}\exp(-\frac{1}{2\sigma^2}\|x_p - c_i\|^2)\ j = 1,2,\cdots,n \tag{8}$$

The loss function using least squares can be expressed as:

$$\sigma = \frac{1}{P}\sum_{j}^{m}\|d_j - y_i c_i\|^2 \tag{9}$$

3.2 Theoretical Analysis of Error Calibration Model

Neural network is a commonly used function fitter. In this paper, the radial basis function in the neural network is used as error compensation. The two-dimensional vector composed of well deflection and azimuth in the modeled data is used as the input vector. The two-dimensional vector consisting of the angle and the azimuth error angle is used as the target vector for training and modeling. The advantage of this method is that it does not need to mathematically model the sensor, nor does it need to know the form of the fitted function, but this method requires a large amount of data to get good accuracy, and the generalization effect is not necessarily good. Therefore, Its disadvantage is that the generalization error is large.

Implemented in MATLAB, you only need to use the newrbe function to design a strict radial basis network. The format in the code is:

net=newrbe（P，T，SPREAD）

Using the radial basis function network to approximate the function, newrbe can quickly design a radial basis network with zero error in the design. Among them: P is the input vector; T is the target vector; SPREAD is the distribution of the radial basis function, and the value when omitted is 1.

3.3 Results of MATLAB Simulation and Error Analysis

The experimental results are shown in Fig 5:

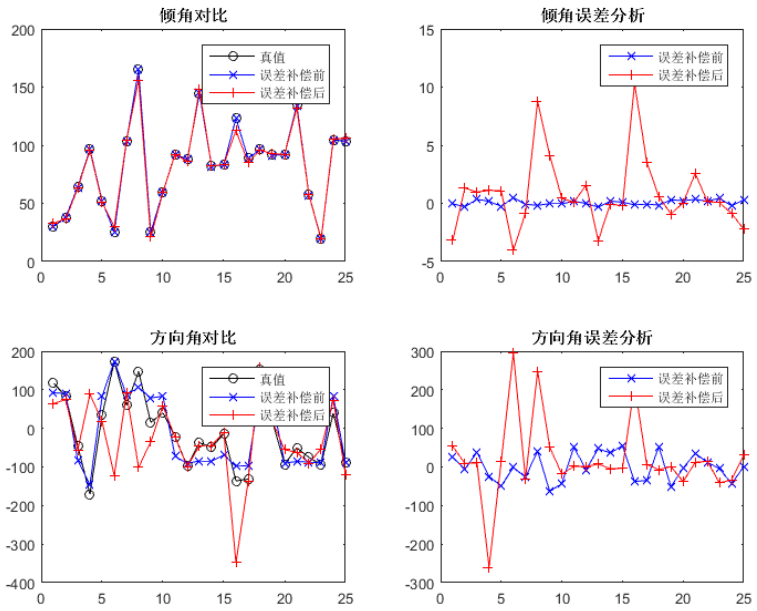

Fig 5 Simulation results based on RBF network

Inclination error: the average value is 2.09152 °; the standard deviation is 2.59812 °; the minimum value is 0.04285 °; the maximum value is 10.29631 °.

Azimuth error: the average value is 56.33606 °; the standard deviation is 90.09415 °; the minimum value is 1.02702 °; the maximum value is 294.996762 °.

It can be seen that the error corrected by RBF is not ideal, and the generalization error is large. Here only 100 data are used to train the network, and 25 data are used for testing.

4. Compensation method based on minimum tilt and azimuth errors

In order to solve the shortcomings of poor generalization performance of RBF and minimize the inclination and azimuth errors, the error compensation can be directly aimed at minimizing the inclination and azimuth errors. In order to improve the accuracy of the model, this paper uses two different optimal solutions to minimize system errors, and uses internal reflection Newton method and sequential quadratic programming algorithm to solve these problems.

4.1 Accelerometer and Geomagnetic Field Model

(1) Sensor model

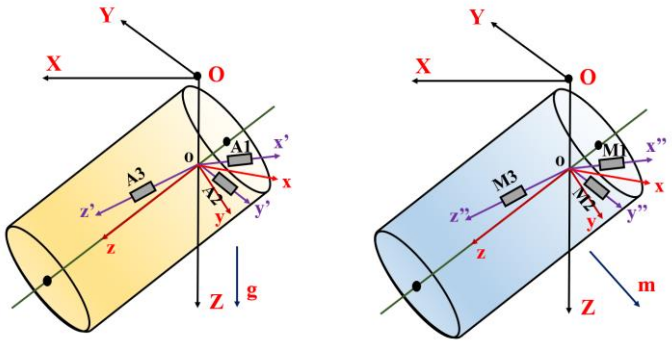

(a) Gravitational model (b) Geomagnetic model

Fig 6 Sensor model. (a) Sensor model in the gravity field, A1, A2, A3 are MEMS accelerometers, g is the gravity vector. (b) Sensor model in the geomagnetic field, M1, M2, and M3 are fluxgate sensors, and m is the geomagnetic vector

As shown in FIG. 6 (a), in the XYZ rectangular coordinate system, the Z axis is the same as the direction of gravity g, and the XOY plane is perpendicular to g. In the xyz rectangular coordinate system in the inclinometer, the z axis is perpendicular to xoy, and the three accelerometers A1, A2, and A3 should be installed along the three axes of the xyz coordinate system, respectively. However, the sensitive axis of the accelerometer is usually not exactly the same orientation during installation. We represent the normalized actual accelerometer output as $G' = [g_{x'}, g_{y'}, g_{z'}]^T$, and the acceleration vector in the ideal xyz coordinate system as $G = [g_x, g_y, g_z]^T$. Describe the accelerometer output as a matrix:

$$G = S(G' - O_g) \tag{10}$$

Where S is a 3 × 3 sensitivity matrix and $O_g = [O_{gx}, O_{gy}, O_{gz}]^T$ is the offset. The diagonal elements of S represent scale factors along three axes, while the other elements of S are called horizontal axis factors. For ideal accelerometers, the horizontal axis factors should all be equal to zero, while for real accelerometers, they can be as high as 2% of the sensor sensitivity.

To further determine the relationship between G and G', rewrite equation (10) as:

$$G' = S^{-1}G + O_g \tag{11}$$

According to the actual physical meaning, we can draw the following conclusions:

$$g_{x'} = k_{gx}[\cos\varphi_{x'x}g_x + \cos\varphi_{x'y}g_y + \cos\varphi_{x'z}g_z] + O_{gx} \tag{12}$$

$$g_{y'} = k_{gy}[\cos\varphi_{y'x}g_x + \cos\varphi_{y'y}g_y + \cos\varphi_{y'z}g_z] + O_{gy} \tag{13}$$

$$g_{z'} = k_{gz}[\cos\varphi_{z'x}g_x + \cos\varphi_{z'y}g_y + \cos\varphi_{z'z}g_z] + O_{gz} \tag{14}$$

Among them, k_{gx}, k_{gy} and k_{gz} are the scaling factors of the three accelerometer sensitive axes, φ is the angle between the three acceleration axes and the three accelerometer sensitive axes, and O_{gx} , O_{gy}, O_{gz} are the offsets of the sensitive axes of each accelerometer. We can see that each actual output of the accelerometer is decomposed into the sum of the projections of the three gravity component vectors, and then a linear error of the form k (·) + O is added to the sum. Then equation (11) can be rewritten as:

$$G' = K_gG + O_g \tag{15}$$

among them

$$K_g = \begin{bmatrix} k_{gx}\cos\varphi_{x'x} & k_{gx}\cos\varphi_{x'y} & k_{gx}\cos\varphi_{x'z} \\ k_{gy}\cos\varphi_{y'x} & k_{gy}\cos\varphi_{y'y} & k_{gy}\cos\varphi_{y'z} \\ k_{gz}\cos\varphi_{z'x} & k_{gz}\cos\varphi_{z'y} & k_{gz}\cos\varphi_{z'z} \end{bmatrix} \tag{16}$$

Since we need the orthogonal acceleration vector in the xyz coordinate system to calculate the parameter system of the inclinometer, we can get it by the following formula:

$$G = [g_x, g_y, g_z]^T = K_g^{-1}(G' - O_g) \tag{17}$$

From the above formulas and processes, it can be seen that the sensor model in this section is similar to the model in section 3.2. The main difference is that K_g^{-1}, K_g^{-1} is obtained from equations (12)-(14), that is, Say, decompose each actual output of the accelerometer into the sum of the projections of the three gravity component vectors, and then derive three ideal orthogonal gravity components from the sensor model.

As shown in Fig 6 (b), the model is the same as the model of the accelerometer, and it is also a problem of coordinate transformation, which is not repeated here.

$$M = [m_x, m_y, m_z]^T = K_m^{-1}(M'' - O_m) \tag{18}$$

4.2 Design of the objective function

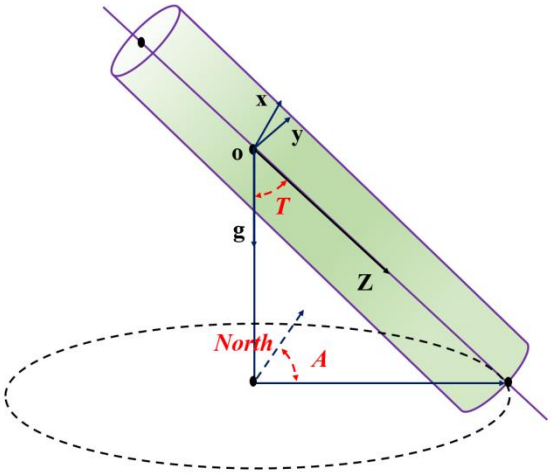

Fig 7 Schematic diagram of tilt angle and azimuth (T represents the tilt angle, A represents the azimuth angle)

The inclination and azimuth are the most important parameters for determining the exact position of the inclinometer and making further work decisions. As shown in Fig. 7, the tilt angle is an angle formed by the z-axis and the downward direction g. The tilt angle is 0 ° when the z-axis is down, and the tilt angle is 90 ° when the z-axis is horizontal. The azimuth is the angle measured from magnetic north (clockwise from above) to the projection of the z-axis on the horizontal plane. Assuming that $G = [g_x, g_y, g_z]^T$ and $M = [m_x, m_y, m_z]^T$ are ideal orthogonal accelerations and magnetic vectors, respectively, the inclination angle (T)[13] and azimuth angle (A)[14] are defined as:

$$T = \arctan\frac{\sqrt{g_x^2+g_y^2}}{g_z} \tag{19}$$

$$A = \arctan\frac{(m_y g_x - m_x g_y)g}{m_z(g_x^2+g_y^2) - m_x g_x g_z - m_y g_y g_z} \tag{20}$$

Generally, many models use the output of the sensor directly to calibrate the sensor. In this paper, we use the minimization of the inclination and azimuth as the optimization goals, and use two kinds of optimization goals for both angles, one is the simple least squares, and the other is the minimization of the maximum error.

(1)Tilt angles

Place the instrument at N_t random positions within the measurement range of the inclination (0 °, 120 °), and record the sensor output $g_{x'}$, $g_{y'}$, $g_{z'}$ and the actual inclination angle T_0, while keeping the instrument under strict static conditions. The error of the tilt is defined as:

$$e_t = |T - T_0| \tag{21}$$

Where T is calculated from equation (19), and g_x, g_y and g_z are obtained from equation (17).

The two optimization goals are:

$$P_g(K_g, O_g) = \operatorname{argmin}\sum_{i=1}^{N_t} e_{t,i}^2 = \operatorname{argmin}\sum_{i=1}^{N_t}|T_i - T_{0,i}|^2 \tag{22}$$

$$P_g(K_g, O_g) = \operatorname{argmin}\left(\max_{i=0}^{N_t} e_{t,i}\right) = \operatorname{argmin}\left(\max_{i=0}^{N_t}|T_i - T_{0,i}|\right) \tag{23}$$

Among them, T_i and $T_{0,i}$ are the calculated and actual tilt angles, respectively. Eq. Is a typical least squares optimization problem, which is expressed as Method I, and the problem is solved using Trust-Region-Reflective algorithm, which is a subspace confidence region method based on internal mapping Newton's method[15]. Minimizing the system's maximum error is the key to accurate

calibration. If the device excels in most positions but exhibits unexpected performance in some special postures, we consider it unqualified. Therefore, another method is proposed to calculate the model parameters and express it as Method II, such as. A typical iterative method, a sequential quadratic programming (SQP)[16] algorithm, is used to solve this problem.

(2)Azimuth angles

Similarly, the azimuth error is defined as:

$$e_a = |A - A_0| \tag{24}$$

Where A is calculated by equation (20), m_x, m_y, and m_z are obtained by equation (18), and A_0 is the actual azimuth of the record. At the same time, place the device at N_a random positions within the measurement range of azimuth (0 °, 360 °) (keep the tilt angle greater than 9 °), and record the sensor output $g_{x'}$, $g_{y'}$, $g_{z'}$, $m_{x''}$, $m_{y''}$, $m_{z''}$, and the actual azimuth A_0. The two optimization goals are:

$$P_m(K_g, O_g, K_m, O_m) = \operatorname{argmin} \sum_{i=1}^{N_a} e_{a,i}^2 = \operatorname{argmin} \sum_{i=1}^{N_a} |A_i - A_{0,i}|^2 \tag{25}$$

$$P_m(K_g, O_g, K_m, O_m) = \operatorname{argmin} \left(\max_{i=0}^{N_a} e_{a,i} \right) = \operatorname{argmin} \left(\max_{i=0}^{N_a} |A_i - A_{0,i}| \right) \tag{26}$$

Similarly, internal mapping Newton method and sequential quadratic programming method are used to solve these problems.

4.3 Results of MATLAB Simulation and Error Analysis

First you need to calculate the parameters of the model, initialize all the parameters, take the output values of the accelerometer and geomagnetic meter, the true values of the inclination and azimuth as inputs, and use the two model parameters $P_g(K_g, O_g)$, $P_m(K_g, O_g, K_m, O_m)$ as the output. Then take model parameter $P_g(K_g, O_g)$ as input and tilt angle as output, calculate acceleration vector $[g_x, g_y, g_z]^T$ by formula (17), and finally calculate tilt angle T according to formula (19); Taking model parameter $P_m(K_g, O_g, K_m, O_m)$ as input and azimuth as output, the acceleration vector $[g_x, g_y, g_z]^T$ and magnetic vector $[m_x, m_y, m_z]^T$ are calculated by equations (17) and (18) respectively, and finally the azimuth angle A is calculated according to equation (20).

The corresponding calculation results and simulation results are as follows.

$P_g(K_g, O_g)$ parameter required by method I:

$$K_g = \begin{bmatrix} 9.8031 & 0.0314 & -0.0016 \\ 0.0314 & 9.7955 & -0.0445 \\ -0.0016 & -0.0445 & 9.8040 \end{bmatrix}, \quad O_g = \begin{bmatrix} 0.0098 \\ 0.0053 \\ 0.0021 \end{bmatrix} \tag{27}$$

The simulation results are shown in Fig 8:

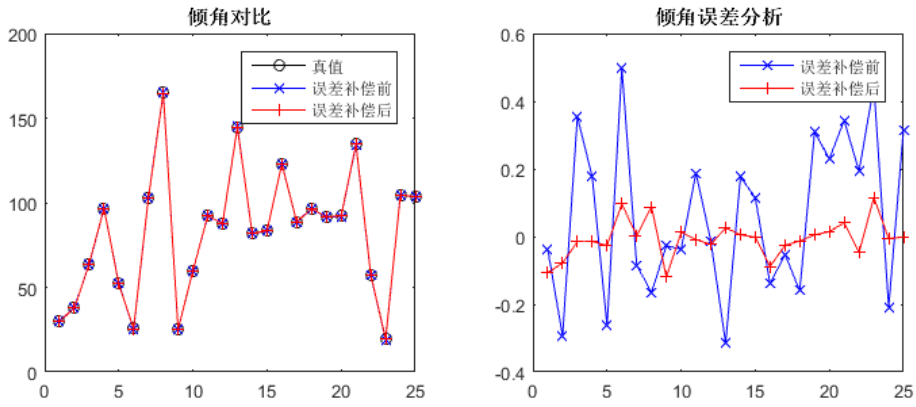

Fig. 8 Simulation results of $P_g(K_g, O_g)$ parameters obtained by method I

Tilt angles error: the average value is 0.03927 °; the standard deviation is 0.04025 °; the minimum value is 0.00090 °; the maximum value is 0.11921 °.

$P_m(K_g, O_g, K_m, O_m)$ parameter required by method I:

$$K_g = \begin{bmatrix} 14.8416 & 0.0389 & -0.0161 \\ 0.0389 & 14.8381 & -0.0285 \\ -0.0161 & -0.0285 & 9.9088 \end{bmatrix},\ O_g = \begin{bmatrix} 0.0101 \\ 0.0050 \\ 0.0018 \end{bmatrix} \tag{28}$$

$$K_m = \begin{bmatrix} 0.8600 & 0.0020 & -0.0004 \\ 0.0020 & 0.8601 & -0.0025 \\ -0.0004 & -0.0025 & 0.5734 \end{bmatrix},\ O_m = \begin{bmatrix} 0.1543 \\ 0.0770 \\ 0.0309 \end{bmatrix} \tag{29}$$

The simulation results are shown in Fig 9:

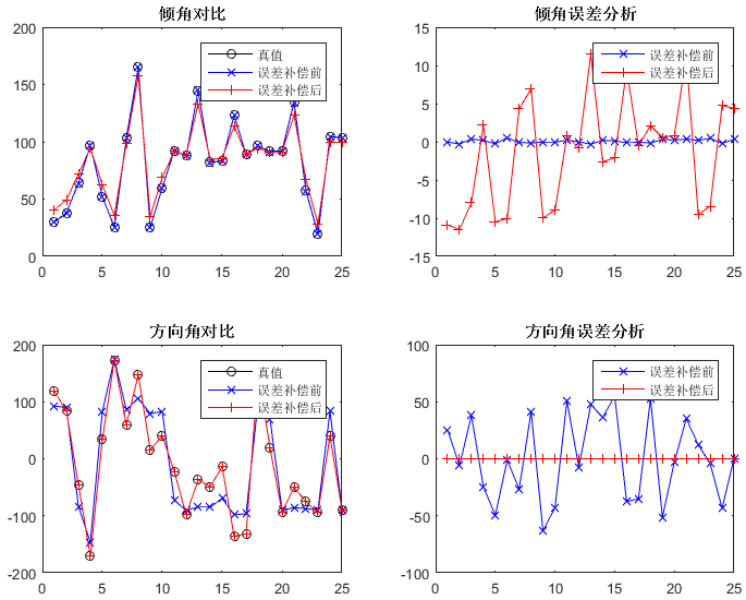

Fig. 9 Simulation results of $P_m(K_g, O_g, K_m, O_m)$ parameters obtained by method I

Tilt angles error: the average value is 6.11278 °; the standard deviation is 4.13938 °; the minimum value is 0.53819 °; the maximum value is 11.51701 °.

Azimuth angles error: the average value is 0.02861 °; the standard deviation is 0.01925 °; the minimum value is 0.00303 °; the maximum value is 0.06476 °.

$P_g(K_g, O_g)$ parameter required by method II:

$$K_g = \begin{bmatrix} 9.8090 & 0.0308 & -0.0073 \\ 0.0308 & 9.7961 & -0.0361 \\ -0.0073 & -0.0361 & 9.7948 \end{bmatrix},\ O_g = \begin{bmatrix} 0.0102 \\ 0.0051 \\ 0.0021 \end{bmatrix} \tag{30}$$

The simulation results are shown in Fig 10:

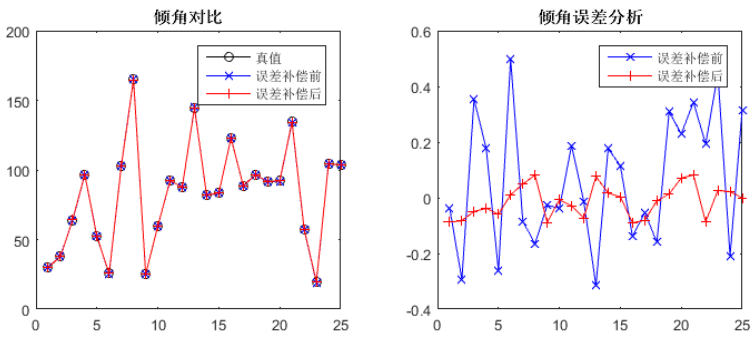

Fig. 10 Simulation results of $P_g(K_g, O_g)$ parameters obtained by method II

Tilt angles error: the average value is 0.04940 °; the standard deviation is 0.03260 °; the minimum value is 0.00116 °; the maximum value is 0.08969 °.

$P_m(K_g, O_g, K_m, O_m)$ parameter required by method II:

$$K_g = \begin{bmatrix} 9.7963 & 0.0226 & -0.0126 \\ 0.0226 & 9.8068 & -0.0174 \\ -0.0126 & -0.0174 & 9.9188 \end{bmatrix}, \quad O_g = \begin{bmatrix} 0.0100 \\ 0.0050 \\ 0.0017 \end{bmatrix} \tag{31}$$

$$K_m = \begin{bmatrix} 0.6484 & 0.0016 & -0.0006 \\ 0.0016 & 0.6485 & -0.0023 \\ -0.0006 & -0.0023 & 0.6552 \end{bmatrix}, \quad O_m = \begin{bmatrix} 0.1542 \\ 0.0771 \\ 0.0308 \end{bmatrix} \tag{32}$$

The simulation results are shown in Fig 11:

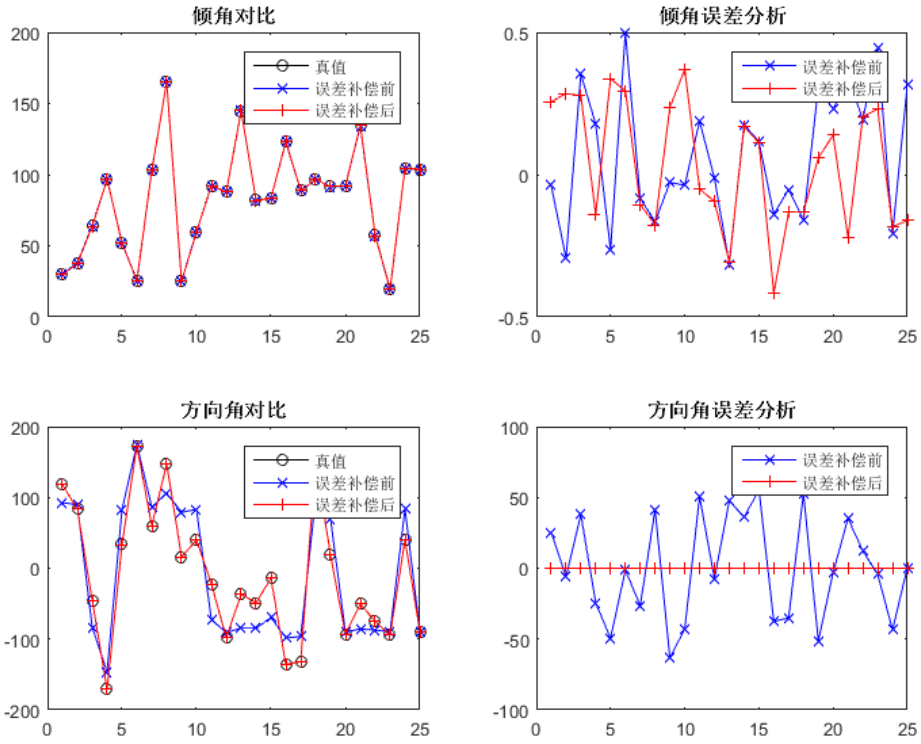

Fig. 11 Simulation results of $P_m(K_g, O_g, K_m, O_m)$ parameters obtained by method II

Tilt angles error: the average value is 0.20359 °; the standard deviation is 0.09658 °; the minimum value is 0.05101 °; the maximum value is 0.41679 °.

Azimuth angles error: the average value is 0.06388 °; the standard deviation is 0.02807 °; the minimum value is 0.00416 °; the maximum value is 0.10039 °.

5. Summary

The error model established by the RBF neural network has a fast calculation speed and does not need to know the error distribution rule in advance. It avoids the analysis of complex actual measurement systems and some test work, but it can be seen from the simulation results that the generalized error comparison Large, if you want to reduce the error, you must train a large amount of data to ensure accuracy, and there are certain limitations in the application. While the error compensation is aimed at minimizing the inclination and azimuth errors, it can be seen that the effect of error compensation is very obvious. Compared with the RBF neural network, the accuracy of the inclination and azimuth errors has been greatly improved. It provides a reference method for error compensation of downhole inclinometer in oil well application.

References

[1] Heping Tan. Research on Drilling Technology of Long Displacement Horizontal Well [J]. China Petroleum and Chemical Standards and Quality, 2014(8), p. 175.

[2] Qinglong Liu. Development of Simple Wireless Logging While Drilling Tool [D]. Xi'an：Xi'an Jiaotong University, 2001, p. 1-2.

[3] Zaiko A I, Ivanova G A. An Inclinometer System for Underground Spatial Orientation[J]. Measurement Techniques, 2014, p. 812-817.

[4] Chengli Wang, CHIKHOTKIN V F, Chunhua Lu. Experimental Study on Error Compensation of Inclinometer While Drilling [J]. Coal Geology and Exploration, 2016, p. 147-151.

[5] Wei Wu. Measuring principle and mathematical model of magnetic inclinometer [J]. Inertial navigation and instrumentation, 1996, p. 52-55.

[6] Zhang Y, Wang Y, Li H. The azimuth error compensation for inclinometer based on gyrocompass[C]//Seventh International Symposium on Instrumentation and Control Technology: Measurement Theory and Systems and Aeronautical Equipment. International Society for Optics and Photonics, 2008, 7128: 71280T.

[7] Renxia Xue. Application of gravity accelerometer in tilt measurement [J]. Sensor Technology, 1998,17(2), p. 40-45.

[8] Zhiwei Wang. Application of Accelerometer and Flux Gate in Directional Probe [J]. Western Exploration Project, 2018, p. 26-28, 30.

[9] Yubo Zhang, Yaohua Meng, Chunming Wei. Research on Sensor Signal Processing Technology in MWD Inclinometer [J]. Journal of Kunming University of Science and Technology (Science and Technology), 2010, 35(2), p. 72-73.

[10] Broomhead D S, Lowe D . Multivariable Functional Interpolation and Adaptive Networks[J]. Complex Systems, 1988, 2(3), p. 321-355.

[11] Moody J, Darken C J . Fast Learning in Networks of Locally-Tuned Processing Units[J]. Neural Computation, 1989, 1(2), p. 281-294.

[12] Rovithakis G A. Robust neural adaptive stabilization of unknown systems withmeasurement noise[J]. IEEE Transactions on Systems Man & Cybernetics Part B Cybernetics, 1999, 29(3), p. 453-459.

[13] Frosio I, Pedersini F , Borghese N A . Autocalibration of Triaxial MEMS Accelerometers With Automatic Sensor Model Selection[J]. IEEE Sensors Journal, 2012, 12(6), p. 2100-2108.

[14] Zhu R, Zhou Z , Li S , et al. A novel miniature azimuth-level detector based on MEMS[C]// Microelectromechanical Systems Conference. IEEE, 2002.

[15] Steihaug, Trond. The Conjugate Gradient Method and Trust Regions in Large Scale Optimization[J]. Siam Journal on Numerical Analysis, 1983, 20(3), p. 626-637.

[16] Gill P E, Saunders M M A . SNOPT: An SQP Algorithm for Large-Scale Constrained Optimization[J]. SIAM Review, 2005, 47(1), p. 99-131.